Int. J. Heat Mass Transfer. Vol. 19, pp. 71–85. Pergamon Press 1976. Printed in Great Britain

ONSET OF INSTABILITY IN A FLUID LAYER HEATED SINUSOIDALLY FROM BELOW

R. G. FINUCANE
Hughes Aircraft Company

and

R. E. KELLY
Department of Mechanics and Structures,
University of California at Los Angeles, CA 90024, U.S.A.

(*Received* 1 *November* 1974)

Abstract—The problem under investigation is the effect of thermal modulation on the stability of a fluid layer heated from below. An experiment was performed in which a layer of air was subjected to sinusoidal heating about a nonzero mean. A numerical analysis of the linear stability equations indicated that the linear assumption is invalid at the low frequencies of modulation studied experimentally. A nonlinear analysis employing the shape assumption and free boundary conditions was developed and examined numerically. It was found both experimentally and analytically that for low frequencies the modulation is destabilizing, whereas at higher frequencies some stabilization is apparent.

NOMENCLATURE

a, wave number;
A, B, C, temperature amplitudes (4.24);
d, fluid layer depth;
g, gravitational acceleration;
k, m, n, integers;
Pr, Prandtl number;
R, Rayleigh number;
Re, real part;
T, temperature;
t, time;
x, y, z, space coordinates;
u, v, w, velocity components;
$\mathbf{v}$, velocity vector;
V, probe velocity.

Greek symbols

ν, kinematic viscosity;
ε, amplitude of oscillation;
ω, frequency of oscillation [nondimensional];
Ω, frequency of oscillation [dimensional];
κ, thermal diffusivity;
β, thermal gradient;
∇^2, Laplacian operator;
ϕ, angular position;
θ, $T - T_m$;
χ, departure from sine curve;
Δ, difference;
ρ, density;
$\gamma_1, \gamma_2, \gamma_3$, nondimensional qualities (4.9);
$\nabla_\perp$, horizontal derivative;
θ_1, departure from mean temperature;
ψ, nondimensional stream function;
$\tilde{\theta}_2$, convection component (4.19).

Subscripts

c, critical;
p, periodicity criterion;
0, initial conditions;
m, mean.

Superscripts

$*$, dimensional quantity;
$\hat{}$, amplitude;
$\bar{}$, horizontal average.

1. INTRODUCTION

THIS paper concerns the stability of a layer of fluid when heated from below in a periodic manner with time. It is known that the stability of many physical systems may be strongly influenced by temporal modulation of an appropriate parameter. Closely allied mathematically to the present case is the problem of circular Couette flow, i.e. the flow between two coaxially rotating cylinders, when the inner cylinder has a velocity which varies periodically with time. Previous experimental results of Donnelly [1, 2] have indicated that a viscous fluid is stabilized, in the sense that some *averaged* disturbance amplitude can be less for the modulated case, with the degree of stabilization rising from zero at high frequency to a maximum at a frequency of $0{\cdot}274(\nu/d^2)$, where d is the gap between the cylinders and ν is the kinematic viscosity. However, due to experimental limitations, behavior at very low frequencies was not clearly established, although this is precisely the regime for which the *instantaneous* response might be of greatest importance, as will be discussed later. Thompson [3] has presented numerical and experimental evidence that oscillating the inner cylinder about a zero mean results in maximum

stabilization at high frequency, decreasing monotonically as frequency goes to zero. No experimental results other than those presented here exist, to the authors' knowledge, for the case of thermally modulated convection, although Bénard type problems with various types of thermal modulation have received considerable analytical attention. For the present case of modulation at the lower surface, Venezian [4] found that the modulation would be stabilizing, with maximum stabilization occurring as the frequency goes to zero. The analytical approach was a linear perturbation analysis with quantities expanded in powers of amplitude of oscillation ε, assumed to be small. Rosenblat and Herbert [5] investigated the linear stability by expanding in powers of the nondimensional frequency of oscillation ω, at arbitrary amplitude. ($\omega = \Omega d^2/\kappa$, where Ω is the dimensional frequency, d is the depth of the fluid layer, and κ is the thermometric conductivity.) The free-free boundary conditions were used in both of these analyses. Rosenblat and Tanaka [6] used a Galerkin procedure to solve the linear problem when the lower wall temperature is being modulated at finite amplitude and frequency and employed the more realistic rigid wall boundary conditions.

A basic feature shared in part by [4–6] is the utilization of a certain condition, based on Floquet theory, to delineate the stability boundaries, namely, the periodicity condition: if an infinitesimal disturbance achieves net growth over one cycle of oscillation, the state is unstable. Given enough cycles, the disturbance will grow to finite size. The *periodicity criterion* is a sufficient condition for instability, but from an observational and practical viewpoint, it must be considered more carefully. Even if an infinitesimal disturbance has no net growth over a cycle, it is possible that it has grown to finite size during the unstable part of the cycle and then decayed. Hence the heat transfer, for instance, will be significantly different from that predicted by the conductive solution during parts of the cycle.

Similar remarks may be made even if the full nonlinear equations are used. An initially small but finite disturbance may exhibit net decay over a cycle yet still produce observable motion and an increase in heat transport during some part of the cycle. In a real experiment it is irrelevant if a *particular* disturbance decays over many cycles, because naturally occurring background noise will give rise to new disturbances and observed motion continuously.

Some results of the investigations reported in [9–11] are presented in Figs. 1 and 2, where the periodicity condition is used to solve for an upper bound of stable states. In these figures ω is the nondimensional frequency, ε the nondimensional amplitude of modulation, a is the wave number, and Pr the Prandtl number. On the vertical axis, R_c is the critical Rayleigh number of the unmodulated problem according to linear theory, while R_p is the critical Rayleigh number in the modulated case as determined by the periodicity criterion. These figures indicate that $R_p > R_c$ and that maximum stabilization occurs as $\omega \to 0$, rather than at some

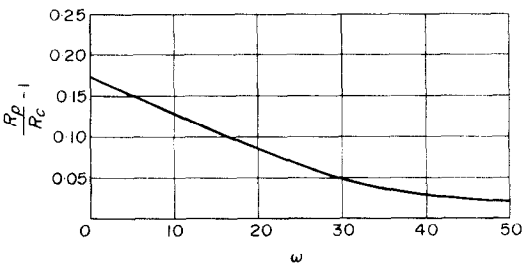

FIG. 1. Variation of critical Rayleigh number with frequency according to the periodicity condition, with $Pr = 1$, $\varepsilon = 1$, $a = 3{\cdot}1$ [4].

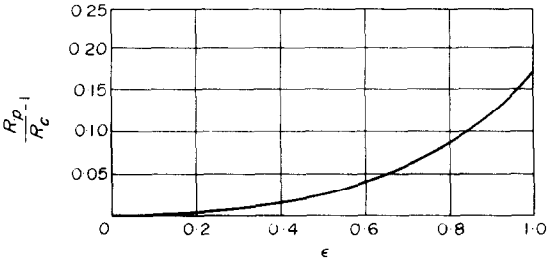

FIG. 2. Variation of critical Rayleigh number with amplitude of modulation, with $\omega = 1$, $Pr = 1$, $a = 3{\cdot}1$ [5].

finite frequency as observed in the Couette flow analog by Donnelly [1]. In view of the doubtful validity of the periodicity criterion when used in conjunction with linear theory and low frequency of modulation, Rosenblat and Herbert [5] propose the amplitude condition, which describes as unstable any disturbance which increases during the cycle by an arbitrary factor of ten. The upper bound in Rayleigh number determined by this criterion is presented in Fig. 3. For comparison, the periodicity condition results for the same boundary conditions are included on Fig. 3 to show the two criteria intersecting at $\omega \approx 3$ when

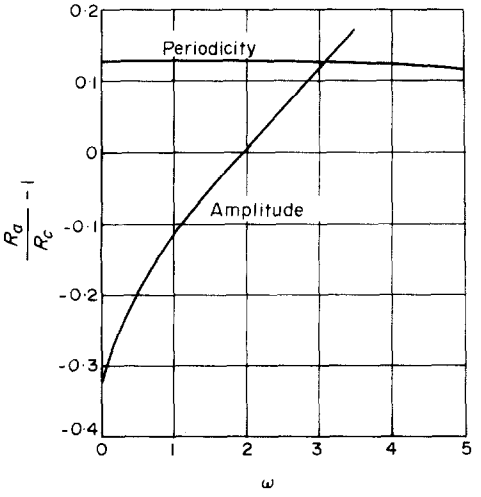

FIG. 3. Comparison between critical Rayleigh number as given by the periodicity and amplitude conditions, with $\varepsilon = 0{\cdot}5$, $Pr = 1$, $a = 3{\cdot}1$ [5].

$\varepsilon = 0{\cdot}5$. Thus the amplitude condition serves the double purpose of describing the qualitative behavior at low frequency and indicating the minimum frequency for which linearization is valid.

The object of the present experiment is to investigate the effects of frequency and amplitude of oscillation on the critical Rayleigh number of the fluid layer. Rather than choosing a criterion for the onset of instability, the experimental results are first presented from an observational point of view. The same spirit is used in the analytical investigation—the behavior of the fluid under a given set of boundary conditions is followed numerically as a function of time. In this way, an attempt is made to describe curves in the ε–ω plane which define the stability in a realistic manner.

2. THE BASIC STATE OF UNSTEADY CONDUCTION

A fluid layer is confined between two horizontal walls separated by a distance d and of infinite horizontal extent. The upper wall has zero temperature, and at the lower wall

$$T^* = \beta d(1+\varepsilon\cos\Omega t^*). \tag{2.1}$$

T^* is temperature, β the thermal gradient, ε the amplitude, Ω the frequency of modulation, and t^* is time. The asterisk denotes a dimensional quantity. In the basic state, before the onset of convection, the thermal profile of the layer is governed by the diffusion equation. With scaling d for length, d^2/κ for time, and βd for temperature, the equations and boundary conditions may be written in nondimensional form:

$$\frac{\partial T_0}{\partial t} = \nabla^2 T_0 \tag{2.3}$$

$$\begin{aligned} T_0 &= 0 \qquad & z &= 1 \\ T_0 &= 1+\varepsilon\cos\omega t \qquad & z &= 0 \end{aligned} \tag{2.4}$$

where

$$\omega = \Omega d^2/\kappa.$$

The solution for T_0 is

$$T_0 = 1-z+Re\left\{\frac{\sinh((1-z)(1+i)(\omega/2)^{1/2})\varepsilon\, e^{i\omega t}}{\sinh((1+i)(\omega/2)^{1/2})}\right\} \tag{2.5}$$

where Re denotes the real part, or

$$T_0 = A\varepsilon\cos(\omega t+\phi)+(1-z)$$

where $A(z)$ is the amplitude and $\phi(z)$ is the phase angle. Figure 4 pictures the temperature at $\omega t = 0$. Included on this figure are same experimental measurements of

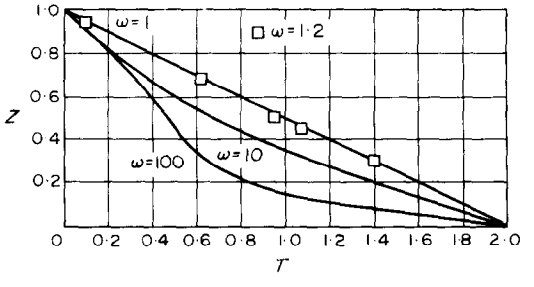

FIG. 4. Static temperature as a function of vertical position, with $\varepsilon = 1$, $t = 0$.

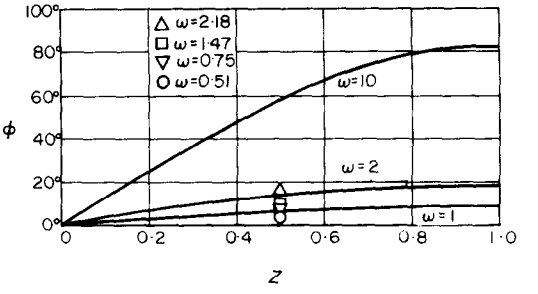

FIG. 5. Phase lag ϕ as a function of vertical position, $\varepsilon = 1$.

peak temperature at $\omega = 1{\cdot}2$, at mean Rayleigh number $R_m = -2100$. On Fig. 5 is plotted the phase lag ϕ as a function of z and $\omega = 1$, 2, and 10. Included are measurements of phase lag taken at the midpoint of the layer, $z = 0{\cdot}5$. Correct quantitative agreement is evident.

The solution for the time dependent temperature profile is presented in detail in the preceding figures to illustrate an important feature of the physical problem at $\omega = O(1)$ or less. At this frequency the temperature gradient is linear, with the numerical results indicating a maximum departure from linearity of the order of one part in 10^3. This conclusion is supported completely by the experimental results, when only small, random variation from a best fit straight line were measured at $\omega \approx O(1)$. The fact that at low frequency the temperature profile is linear suggests a quasi-steady approach to investigating the limit $\omega \to 0$. One argues that if

$$R_{\text{mean}}(1+\varepsilon) > R_c \tag{2.6}$$

convection will occur during part of the cycle for a sufficiently low frequency. R_{mean} is the mean Rayleigh number for modulated lower wall, while R_c is the critical Rayleigh number for the unmodulated problem. The logical justification for the inequality (2.6) is that the left-hand side represents the maximum Rayleigh number attained during the cycle of modulation, which, if the inequality holds, produces an unstable linear gradient in the fluid. It will always be possible to choose an ω low enough that the unstable gradient is maintained long enough for convection to appear. Thus for any ε the critical mean Rayleigh number is seen to be, in the limit $\omega \to 0$,

$$R_m = \frac{R_c}{1+\varepsilon}. \tag{2.7}$$

A low frequency modulation will be destabilizing; for $\varepsilon = 1$ this destabilization amounts to 50 per cent. This conclusion is supported by the experimental investigation, which typically shows measurable convection occurring at the peak of the cycle and disappearing as the lower wall temperature decreases. This intuitive criterion for stability has recently been confirmed rigorously by Homsy [7], who used the energy method to investigate analytically the stability of the case studied here.

3. EXPERIMENTAL INVESTIGATION

3.1. *Experimental apparatus*

The experimental arrangement is composed of the convection chamber containing air and associated instrumentation, the mechanical drive which produces a sinusoidal heat flux, the cooling baths for maintaining upper and lower surface temperatures, and the various recording and measuring devices which provide instrument readout.

The convection chamber itself is depicted schematically in Fig. 6. The chamber is bounded in the horizontal directions by a 20·0 c square of adjustable height. Since the maximum height used is 2·5 c, the minimum aspect ratio is 8:1. Davis [8] has shown that for an aspect ratio larger than 6:1, the critical Rayleigh number should be similar to that of an infinite layer.

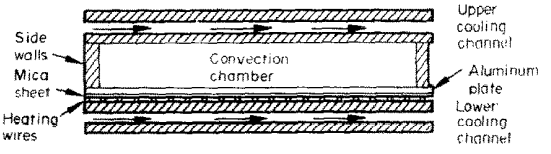

FIG. 6. Schematic diagram of convection chamber.

The upper wall, which is kept at constant temperature, is formed by a glass plate, itself the lower plate of the upper cooling bath. The lower surface of the chamber is a machined aluminum plate, whose temperature is controlled by two independent systems. The first of these is a 0·005-in dia stainless steel wire, strung at intervals of 0·5 in and electrically heated in a manner which produces the sinusoidal component of the lower surface temperature. Separating the bare heating wires from the aluminum plate is a 0·015 in sheet of mica which provides electrical and thermal insulation to insure an even distribution in the spanwise temperature of the plate. Below the wires is the lower cooling channel, whose purpose is to maintain the steady component of the lower surface temperature. Four 0·375-in thick plexiglass members, machined to various heights, placed on edge and glued at the corners, form the sides of the chamber.

The upper wall of the air layer is kept at a constant temperature by a Precision Scientific Company Cat. 66600 bath pumping at 1·5 gal/min. This bath is capable of maintaining its water temperature to $\pm 0{\cdot}02^{\circ}C$. At this flow rate, the increase in water temperature due to the heat transferred through the layer of air at a Rayleigh number three times critical ($R \cong 5000$) is computed to be less than $0{\cdot}001^{\circ}C$.

The steady component of the lower wall temperature is maintained by a Neslab Instruments No. 690606 bath with a pumping capacity of 3 gal/min. The maximum spanwise temperature variation in the lower water bath due to the heat lost from the heating wires is about $0{\cdot}01^{\circ}C$ under the worst case of assuming that all the energy is lost to the coolant. No spanwise nonuniformities are observed which are ascribed to this source.

The water from the two cooling baths is pumped through two channels of similar design. The channels are constructed of two 0·125-in thick pieces of plate glass about 15-in square separated by spacers along two edges to form a laminar sheet flow channel 0·125-in high. The assembly is glued together, with a plenum chamber at each end completing the structure.

The oscillating component of the lower wall temperature is produced by the device sketched in Fig. 7. The heating wires are connected to a 0–150 V AC variac whose control knob is cam driven so that its angular position ϕ is given by $\phi \sim \pm |\sin t|^{1/2}$, where t is time, and the minus sign applies when $\sin t < 0$.

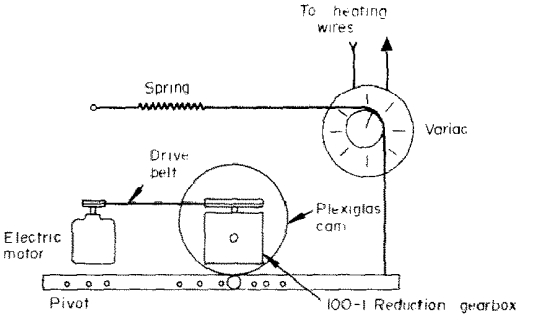

FIG. 7. Mechanism for producing oscillating component of lower wall temperature.

The instrumentation consists of two copper–constantan thermocouples which measure temperature differences between the upper and lower surface and a probe mounted thermistor to determine the local temperature at any point in the convection chamber.

The temperature probe is mounted in an overhead carriage mechanism and driven by a jack screw device to permit linear traversing speeds horizontally through the chamber ranging from 1 mm to 10 cm/min. The jack screw is driven through reduction gearing by a fractional horsepower Bodine synchronous motor.

A moving probe was found to give a much more reliable and repeatable indication of the onset of convection than a stationary one. With no convection present, the stationary and moving probes produce identical sine curves. As convection begins, a stationary probe reveals only a gradual distortion of the curve, whereas a moving probe imposes an additional sine wave of different period whose presence is readily detectable. Care is required to insure that the probe velocity selected is not coincidently equal or nearly equal to the product of modulation frequency and convection roll wavelength; such a probe is effectively stationary.

The thermistor probe itself consists of a 16 in long hollow, stainless steel tube with 0·031 in O.D. Soldered to the tip of the probe was a 0·001-in dia platinum–iridium lead wire of a Fenwall thermistor bead 0·014-in thick. The other thermistor lead wire was soldered to a single strand copper wire insulated with lacquer and inserted in the center of the hollow tube. This arrangement provides a rigid probe of small size and smooth exterior to minimize the disturbance of the working fluid.

The Fenwall bare bead thermistor used has a time constant in still air of 1·7 s. The nominal resistance at 25°C is $15 \times 10^6\,\Omega$, with a coefficient of resistance change with temperature of $-0{\cdot}044$/°C.

A standard thermistor bridge is designed and calibrated against a precision mercury in glass thermometer. It is possible to check the thermistor against the thermocouple by measuring the wall temperature difference with the thermistor, and this measurement is self-consistent to within $\pm 0{\cdot}06$°C. Temperature in the fluid layer as measured by the thermistor is recorded on a Houston Instruments Model 6325 strip chart millivolt recorder. The result is a history of the temperature at a given vertical position as a function of time and horizontal position in the fluid layer.

Output from the thermocouple junction, giving the time dependent boundary conditions of the system, could be read from a Hewlitt–Packard Model 6520 millivoltmeter or recorded directly on the Houston Instruments strip chart recorder. The recorder, however, has only one channel, so that only one temperature can be recorded while the other is visually monitored. The usual procedure is to first record the boundary conditions at the beginning of a run to insure that the desired temperature–time curve is being produced, then record the probe temperature only during the rest of the run. The maxima and minima of the lower wall temperature are then hand written directly onto the chart as the mean temperature, amplitude or frequency is changed.

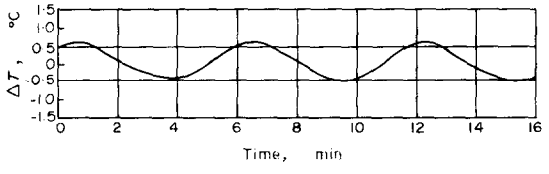

FIG. 8. Temperature difference measured between upper and lower walls as a function of time.

Figure 8 represents the output from the thermocouples giving the temperature difference between the upper and lower walls of the convection chamber. The curve can be seen to be very nearly sinusoidal. The maximum deviation from a cosine curve is 20·5 per cent of amplitude at $\phi = 75°$. The RMS variation defined as

$$\left[\frac{1}{2\pi}\int_0^{2\pi}(\cos\phi - \chi(\phi))^2\,\mathrm{d}\phi\right]^{1/2}$$

is about 7 per cent of amplitude over the whole cycle. These values are typical of those present during the entire experimental program. Occasional larger variations were induced by pulley slippage, spring failure, and other mechanical sources, but data taken under these circumstances are not reported. The source of the observed deviation from the desired sine curve is believed to be the low power output of the fractional horsepower Bodine synchronous motor used to drive the cam. Near the top of the cycle, when the follower return spring was at its maximum extension, the motor was retarded prior to, and accelerated after, the peak. These effects are not considered to have major impact on the experimental results.

Ideally, the experiment should investigate the effect of modulation over the widest possible range of ω and ε, the nondimensional frequency and amplitude, respectively. In particular, it is desirable to vary ω in the range from 1 to 10 or higher, while keeping ε of order 1. The actual performance attainable in the device is $\omega \sim 3$ and $\varepsilon \sim 0{\cdot}30$, with ε varying inversely with ω. The largest frequency attainable at amplitude of order unity is $\omega \sim 2$. The explanation for this poor performance hinges around the thermal behavior of the lower aluminum plate whose temperature is to be sinusoidally modulated to impose the desired boundary conditions upon the layer of fluid.

The lower aluminum plate has two purposes, namely, to smooth out the thermal nonuniformities induced by the discretely spaced heating wires and to uncouple the imposed boundary conditions from the motions induced in the convection chamber. The minimum plate thickness used is 0·080-in thick, whose heat capacity per unit area is $0{\cdot}151\,\mathrm{J/cm^2\,°C}$. The heat flux through the air layer at critical Rayleigh number is $1{\cdot}15 \times 10^{-4}\,\mathrm{W/cm^2}$, which means that the maximum rate of change in temperature of the lower plate due to conduction through the air layer is of the order of 0·014°C/min. At three times critical this increases to about 0·03°C/min [9], still very low in comparison to the imposed temperature difference of the order 1°C.

The other purpose of the lower plate is also accomplished in that no measurable horizontal temperatures are apparent either on the plate itself or in the air layer during subcritical operations. Nor are any instances of flow patterns with wavelength comparable to heating wire spacing ever observed; the usual size of the convection rolls is four to five times wire spacing. However, the fact that only rolls parallel to the heating wires occurred is evidence that a preferred orientation exists, so that a still thinner lower plate may cause significant departure from the ideal boundary conditions.

We now examine how the lower plate limits the performance of the experimental apparatus. During the first half of the cycle of oscillation, when the temperature is decreasing, a quantity of heat must be removed from the system to cause the plate to drop in temperature by an amount

$$T = \frac{\varepsilon \Delta T}{2}$$

where ε is the amplitude of oscillation and ΔT is the imposed temperature difference at $R_c = 1708$. This relation is true when (as in this case) the problem is to be studied when the mean Rayleigh number R_m is to be in the vicinity of R_c. This temperature decrease has to occur in half a cycle of oscillation, or

$$\tau = \tfrac{1}{2}\left(\frac{2\pi}{\Omega}\right) = \frac{\pi}{\Omega},$$

where Ω is the dimensional frequency of oscillation. The

mean slope in the temperature time curve is thus

$$\frac{dT}{d\tau} = \frac{\frac{\varepsilon\Delta T}{2}}{\frac{\pi}{\Omega}} = \frac{\varepsilon\Omega\Delta T}{2\pi}.$$

This slope is fixed by the physical design of the experiment: the plate thickness, the cooling channel, the insulating layers between, and so forth, as has been shown. The heat loss through the fluid layer itself is negligible. We may now write the product which defines system performance,

$$\varepsilon\Omega = \frac{dT}{d\tau}\frac{2\pi}{\Delta T}.$$

In terms of nondimensional frequency

$$\varepsilon\omega = \frac{dT}{d\tau}\frac{2\pi}{\Delta T}\frac{\kappa}{d^2}.$$

The gap spacing is expressible in terms of the Rayleigh number:

$$d = \left(\frac{R_m}{\Delta T}\frac{\kappa\nu}{g\alpha}\right)^{1/3}$$

which leads to

$$\varepsilon\omega = 2\pi\frac{dT}{d\tau}\left(\frac{R_m}{g\alpha}\frac{\nu}{\kappa^{1/2}}\right)^{2/3}\Delta T^{-5/3}.$$

If one wishes to optimize the performance of the system by maximizing the product $\varepsilon\omega$, three avenues of approach are available. First, a working fluid should be chosen whose properties are such that the group

$$\frac{\nu}{\alpha\kappa^{1/2}}$$

is as large as possible. An additional constraint as to the choice of fluid is imposed. Theoretical predictions indicate that the effects of modulation are at a maximum at Prandtl number in the vicinity of unity, falling off rapidly on both sides of the peak. This limits the choice of fluids to air at room temperature and water in the vicinity of its boiling point. The product of properties

$$\frac{\nu}{\alpha\kappa^{1/2}}$$

is more than twice as large for air than for hot water. It is also possible to show that the gap spacing d needs to be very much smaller for water, and the attendant difficulties of dealing with high temperature water need no elaboration. The only reasonable fluid for this investigation thus becomes air.

Assuming $dT/d\tau$ is optimized by clever design of the heating wires, cooling channels, and so forth, one sees that the performance of the system is inversely proportional to $\Delta T^{5/3}$, at a given operating Rayleigh number R_m. In the design of this experiment, it was decided that the minimum practical ΔT for normal operation at $R_m = 1708$ would be $\Delta T \approx 1°C$; below this value, uncontrollable fluctuations of the boundary conditions become too large relative to the imposed temperature difference. The maximum gap size was thereby fixed at $d = 2{\cdot}48$ cm. A carefully designed and controlled future experiment may attain increased performance by operating at a higher gap spacing.

The maximum stabilizing effect predicted theoretically is only about 20 per cent, indicating that R_m will be in the vicinity of 1708. Using this value of R_m, $\Delta T \approx 1°C$, and the experimentally determined maximum $dT/d\tau$, it is found that the greatest performance of the system could be expressed

$$\varepsilon\omega \approx 2.$$

It should be stressed that this is true only at $R_m = 1708$; as $R_m \to 0$, the performance increases without limit for a fixed gap size d.

Experience gained during the course of the experiment, together with the preceding considerations, indicates that the best way to improve system performance is to abandon the heating wires and the attendant necessity for a thick homogenizing plate. Instead, the oscillating component of the boundary temperature could possibly be induced by a motor driven mixer valve which appropriately combines a hot and a cold water supply.

3.2. *Temperature measurements and their interpretation*

The results will be presented in two parts. The first part consists of a series of examples of typical traces, with accompanying commentary setting forth possible interpretations of the observed distortions in the temperature profile. In support of these conclusions, results of the theoretical investigation with similar boundary conditions and probe initial conditions are presented in Section 4.

The second part of the presentation consists of various correlations of the data, giving observed trends with ω, ε, and R_m. Points of agreement and disagreement with previous and present analytical investigations are included. These correlations are given in Section 5.

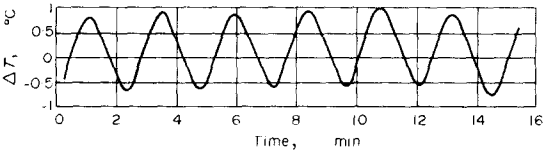

FIG. 9. Temperature trace, with $z = 0{\cdot}5$, $R_{min} = -1400$, $R_{max} = 2040$, $\varepsilon = 5{\cdot}3$, $\omega = 1{\cdot}23$.

Figure 9 is a record of the temperature observed by the 0·014-in dia probe mounted thermistor bead as it travels horizontally through the fluid layer at a vertical position $z = 0{\cdot}5$ and linear traversing speed of 0·207 in/min. The boundary conditions in this example are low enough that no observable motions are induced in the fluid anywhere during the cycle. The variation in peak temperature amounts to 0·145°C and is due to an imposed change in the mean temperature difference. The amplitude and phase lag are 0·96 and 4°, respectively, compared to the theoretical values of 1·0 and 7·1°. This figure is a typical experimental observation of the basic state.

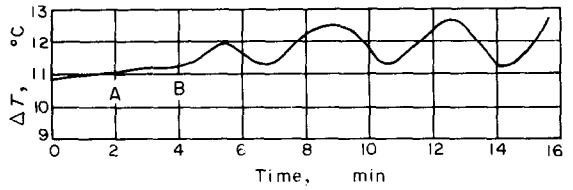

FIG. 10. Temperature trace showing the formation of convection rolls, no modulation, with $z = 0{\cdot}4$.

Figure 10 displays the onset of convection at $\varepsilon = 0$, that is, without modulation. One sees the development of symmetrical rolls of wavelength $1{\cdot}87 \pm 0{\cdot}05$ cm compared to the theoretical value of 1·92 cm. (For this case, a smaller gap width was used than in the following figures.) The Rayleigh number is being gradually increased with time, so that at A, $R = 1620 \pm 85$, while at B, $R = 1670 \pm 85$. The experiment does not produce precision results of critical Rayleigh number in the unmodulated case, but does give a good picture of the remarkable regularity of the thermal distribution within the roll.

Figure 12 shows the flow pattern observed when the maximum Rayleigh number is slightly higher than that of the preceding figure ($R_{max} = 3240$). The physical behavior of the system is typical of that seen during much of the experimental investigation in this frequency range. Observe the points labeled A, B, and C. Point A represents a local downdraft of magnitude 0·16°C which has appeared very near but slightly following the peak of the temperature cycle. One can imagine the probe travelling horizontally and encountering quiescent fluid only until just prior to point A. Upon arrival at A, the probe encounters one edge of a convection cell which appears as the observed depression. The probe continues in space observing fairly uniform, motionless fluid past points E and D until it

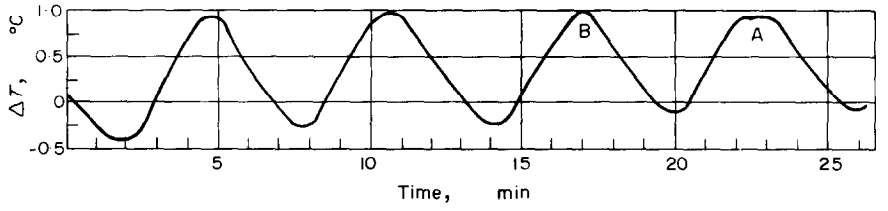

FIG. 11. Temperature trace, with $z = 0{\cdot}5$, $R_{min} = -1570$, $R_{max} = 2220$, $\varepsilon = 5{\cdot}75$, $\omega = 0{\cdot}513$.

Figure 11 shows the temperature recorded by the moving probe when we have modulation and when the mean Rayleigh number is gradually increasing. "Time" in this and subsequent figures refers to the time after the probe has begun to move. R_{min} refers to the minimum Rayleigh number measured, whereas R_{max} refers to the maximum. The trace is typical of that observed as the lower wall undergoes modulation at high amplitude and low frequency and mean Rayleigh number $\varepsilon = 5{\cdot}5$, $\omega = 0{\cdot}513$, $R_{mean} = 325$. Under the conditions of this figure, the thermal gradient is adverse and supercritical from a quasistatic viewpoint for 20 per cent of the cycle, adverse and subcritical for 30 per cent, and favorable for nearly 50 per cent of the time. After about an hour, during which the mean Rayleigh number increases from 320 to 650, the first small evidence of thermal convection begins to appear at the peak of the temperature cycle, when the maximum Rayleigh number is 2550. It can be seen that this evidence consists of a decrease in the temperature of the fluid of the order of 0·03°C at point A, representing the fact that the probe has encountered a slight downdraft of cool fluid from above. Convection also probably occurs previously at point B. The presence of this small amount of convection illustrates a key point in any discussion of the effects of modulation on the stability of the fluid layer: What criterion is to be used to define stability? If one proposes to define as unstable those boundary conditions which

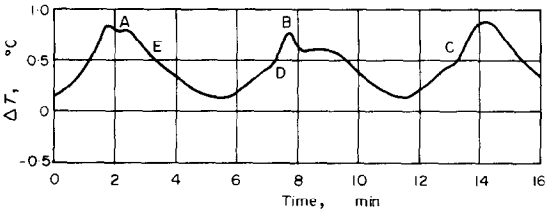

FIG. 12. Temperature trace, with $z = 0{\cdot}5$, $R_{min} = 970$, $R_{max} = 3240$, $\varepsilon = 0{\cdot}595$, $\omega = 0{\cdot}513$.

produce observable motion at any time during the cycle of oscillation, then this figure is an example of instability at $R = R_c/2{\cdot}6$. The whole question of what constitutes stability or instability as the terms are applied to the experimental evidence is discussed in more detail in Section 5.

arrives at B. Point B represents an updraft of roughly 0·256°C magnitude, or about 25 per cent of modulation amplitude. Notice that it occurs significantly prior to the peak in the lower wall temperature, so that the local instantaneous Rayleigh number is about 2600 compared to 3200 at A. Nonetheless, the disturbance at B can be seen to be larger in amplitude than that at A. This effect is commonly seen during the course of the investigation: updrafts appear as larger, more concentrated thermal plumes while downdrafts are more diffuse being lower in magnitude and larger in horizontal extent. Qualitative similar patterns, but of the opposite sense, have been reported by Spangenberg and Rowland [9], in their optical investigation of evaporatively cooled water. Convection in their study appears in the form of plunging sheets of cooled fluid, with warmer updrafts of lower velocity and larger volume. Other types of flow patterns observed in unsteady heating problems are discussed by Currie [10].

The wavelength of the convection cell in Fig. 12 may be determined from points A, B and C. The speed of the probe (0·207 in/min) combined with the speed of the chart (0·500 in/min) gives the moving probe horizontal distance scale: one inch on the paper is equivalent to a probe travel of 1·036 cm. The physical distance between events A and B thus becomes 2·91 cm; the wavelength, or distance between A and C is 5·65 cm. The predicted wavelength of the critical disturbance at $R = R_c$ for the unmodulated case is 5·00 cm.

is closer to the local physical downdraft maximum than A'', while the latter is nearer the temporal maximum. The two effects are additive at D and E, while they partially cancel at A, B and C. Thus what at first glance appears as a fairly random wavy pattern can be seen to contain a surprising amount of detail about the behavior of the system. All of the described effects have been duplicated in the numerical integration of the nonlinear equations governing the motion within the convection chamber.

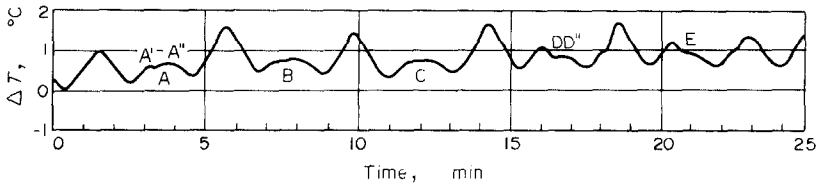

FIG. 13. Temperature trace, with $z = 0{\cdot}5$, $R_{min} = 835$, $R_{max} = 1810$, $\varepsilon = 0{\cdot}54$, $\omega = 1{\cdot}72$.

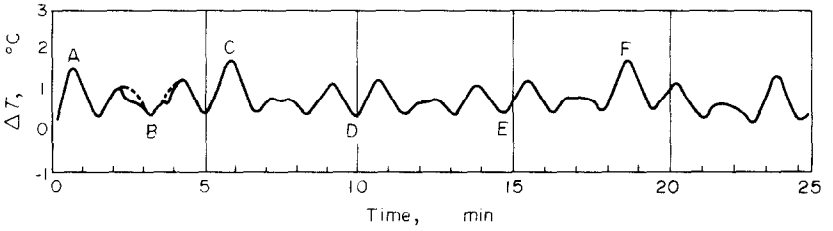

FIG. 14. Temperature trace, with $z = 0{\cdot}5$, $R_{min} = 880$, $R_{max} = 2250$, $\varepsilon = 0{\cdot}55$, $\omega = 1{\cdot}78$.

In Fig. 13 the probe speed and initial position are adjusted so that a cell boundary is intercepted near the peak of every cycle of oscillation. In this and the next figure, one inch on the chart represents 2·2 cm of probe travel in the convection chamber. The adjustment is not precise, as can be seen from the fact that the maximum intensity of the convective downdraft moves from a position left of the peak at A, to a centered position at C, then off to the right of the lower wall maximum at E. The updrafts cause an elongation of the profile at the maxima in between the lettered points. The asymmetry associated with the two local maxima A' and A'', and the opposite asymmetry at D, are explained by the relationship between the physical location of the probe and the temporal cycle of oscillation. The local maximum at A'' is higher than that at A' because at A'' the probe moves from the cell boundary and does not observe the effects of the downwash. Thus, the temperature is nearer its higher conduction value. The actual location of the cell boundary may thus be placed somewhat to the left of A, between A and A'. Similar reasoning places another cell boundary to the right of the minima at D or E. The change in the pattern between C and D is much more pronounced than that between B and C, and the difference in local maxima surrounding D is greater than that in those surrounding A. These phenomena are due to the continuous growth in the convection strength, so that D'' is both close physically to the center of the cell boundary and nearer (temporally) to the instant of maximum velocity. A' on the other hand,

The varying effects produced when the probe passes a given location in a convection cell at different times in the oscillation cycle are graphically illustrated in Fig. 14. Points A and C represent the probe passing through the center of an upwelling of warm fluid at the cell boundary near the maximum in the lower wall temperature. The intervening downdraft would have occurred near B, but at this instant in time the convection has ceased, and the probe measures the conduction temperature only. One sees, however, evidence of the downdraft before it ceases prior to B and after it reappears just after B. This evidence is in the form of a depression from the conduction profile in the amount indicated by the dashed lines.

The next updraft following C should occur at point D. Here again the convection has ceased, so that D is at the same temperature as B, given by the conduction solution. In contrast to the situation at B, no evidence of convection either prior to or following D is apparent. This is another example of the horizontal irregularity of the convection observed in the modulated problem: the updrafts are localized and intense, while the downdrafts are more diffuse. The point C is displaced upward farther from the conduction point than the subsequent downdraft is displaced downward. Updrafts are "missed" by the probe at D and E, but the downdraft is visible in every intervening instance, i.e. between C and D, D and E, and E and F.

The picture of the convective flow pattern presented in Fig. 15 is more complex than that of previous figures. The probe has been slowed so that 1 in on the

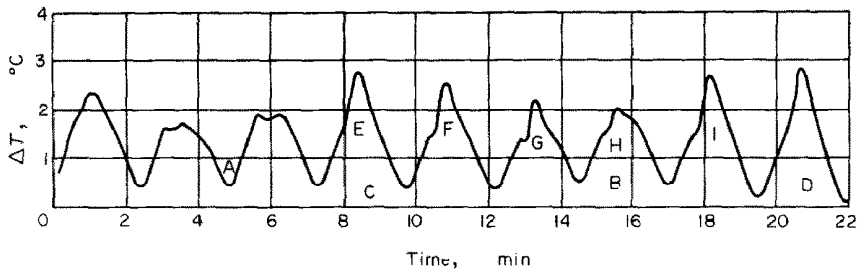

FIG. 15. Temperature trace, with $z = 0{\cdot}5$, $R_{min} = 820$, $R_{max} = 4270$, $\varepsilon = 0{\cdot}68$, $\omega = 1{\cdot}23$.

chart represents 1·036 cm of probe travel. Determination of the convection wave number is not too precise, but one might visualize areas of downdraft centered at A and B, with plumes ascending in the vicinity of C and D. Although the exact location of the cell boundaries is uncertain, the wavelength derived from the distance A–B is 5·6 cm. Of particular interest in this figure are the points labeled E–I. At each of these points, to varying degrees, the slope of the time–temperature curve suddenly decreases. Peculiarities of these bends in the profile are first, that they occur only on the upswing, or increasing part of the cycle, and second, that they are associated not with the convective wave number, but rather with the time scale of the oscillation. The nature of these disturbances was not discovered until they unexpectedly began to turn up in the numerical solution of the energy equations governing the fluid. They are due to the distortion of the mean profile which occurs at the onset of convection. This distortion of the mean, being smaller in magnitude than the fundamental convection mode, is only visible at a null point in the center of a roll where the velocity of the fundamental is zero. One infers that a hysteresis is present in the system which results in a gradual decrease in convection as the Rayleigh number becomes subcritical on the reverse side of the curve. Thus, no sharp bend is present on the downslope side.

In the preceding figures we have presented some of the qualitative behavior observed in the convection chamber. Most of the types of patterns discussed have also been predicted analytically in the relations to be developed in subsequent sections. The main thrust of the observational data, namely, the point of onset of convection and how it varies with the parameters of modulation, is presented in Section 5.

4. STABILITY ANALYSIS

The behavior of the fluid in the convection chamber is governed by the equations of motion, continuity, and energy. Chandrasekhar [11] presents details of the derivation of these relations in the Boussinesq approximation. Retaining only linear terms, the equations may be written in nondimensional form:

$$\frac{1}{Pr}\frac{\partial v}{\partial t} = \frac{1}{Pr}\nabla p + \nabla^2 \mathbf{v} - R\theta \mathbf{k} \tag{4.1}$$

$$\nabla . \mathbf{v} = 0 \tag{4.2}$$

$$\frac{\partial \theta}{\partial t} + \frac{w\partial T_0}{\partial z} = \kappa \nabla^2 \theta. \tag{4.3}$$

In the above expressions, T_0 is the basic conduction temperature given by (2.14), $\theta = T - T_m$, and the hydrostatic pressure has been subtracted. Additional scaling factors are κ/d for velocity and $\rho_m \kappa^2/d^2$ for pressure, with ρ_m being the fluid density at a reference temperature T_m. If one takes the curl twice of equation (4.1), utilizing the solenoidal character of the velocity field (4.2), and some algebra, the vertical component of the linearized equation of motion may be written:

$$\left(\frac{\partial}{\partial t} - \nabla^2\right)\left(\frac{1}{Pr}\frac{\partial}{\partial t} - \nabla^2\right)\nabla^2 w = -\frac{\partial T_0}{\partial z} R \nabla_1^2 w \tag{4.4}$$

θ has been eliminated from (4.4) by using (4.3), and the Prandtl and Rayleigh numbers are

$$Pr = \frac{\nu}{\kappa}, \qquad R = \frac{g\alpha\beta d^4}{\kappa\nu}.$$

The procedure for developing (4.4) is the same as in the unmodulated problem and is covered in [11]. We now Fourier analyze the vertical component of the disturbance velocity in the horizontal plane:

$$w = \hat{w}(z, t)\exp(i(a_x x + a_y y)). \tag{4.5}$$

If $\hat{w}(z, t)$ is furthermore expanded in a Fourier series in z with time dependent coefficients,

$$\hat{w}(z, t) = \sum_{m=1}^{\infty} x_m(t)\sin m\pi z \tag{4.6}$$

it is possible to satisfy the free-free boundary conditions on w:

$$w = \frac{\partial^2 w}{\partial z^2} = \frac{\partial^4 w}{\partial z^4} = 0 \quad \text{at} \quad z = 0, 1. \tag{4.7}$$

If we substitute (4.6) into (4.4), multiply through by $\sin n\pi z$, and integrate with respect to z over the interval $(0, 1)$, the equation for the time dependent coefficient x_n is

$$\frac{d^2 x_n}{dt^2} + (1 + Pr)(n^2\pi^2 + a^2)\frac{dx_n}{dt} + Pr\left((n^2\pi^2 + a^2)^2 - \frac{Ra^2}{n^2\pi^2 + a^2}\right)x_n - \frac{\varepsilon Ra^2 Pr}{n^2\pi^2 + a^2} \times \sum_{m=1}^{\infty} x_m \left\{\frac{2\gamma_1}{\gamma_2^2 + \gamma_3^2}\left[\gamma_3 \cos\omega t - \gamma_2 \sin\omega t\right]\right\} = 0 \tag{4.8}$$

where

$$\begin{aligned} \gamma_1 &= 2\pi^2 mn\omega \\ \gamma_2 &= \pi^4(n-m)^2(n+m)^2 - \omega \\ \gamma_3 &= \omega\pi^2(2n^2 + 2m^2). \end{aligned} \tag{4.9}$$

Equation (4.9) describes the behavior of small velocity disturbances as a function of time. For later comparison to the experimental results, we wish to determine the temperature field as well. The vertical component of the linearized equation of motion gives the desired connection:

$$\frac{\partial}{\partial t}\nabla^2 w = g\alpha(\nabla_1\theta) + \nu\nabla^4 w. \tag{4.10}$$

The observed convection mode was two dimensional rolls induced by the heating wires as discussed in Section 3.

If we take the horizontal dependence of θ as

$$\theta = \theta(z,t)\cos ax \tag{4.11}$$

then, by substituting into (4.10) and using the previous Fourier expansion for $w(z,t)$, we obtain

$$\theta = \frac{\cos ax}{Ra^2}\sum_{m=1}^{\infty}(m^2\pi^2+a^2)(\sin m\pi z) \times\left((m^2\pi^2+a^2)x_m + \frac{1}{Pr}\frac{\partial x_m}{\partial t}\right). \tag{4.12}$$

We wish to simulate the temperature measured by a probe moving perpendicular to the longitudinal axis of the two dimensional roll. It is also convenient to be able to adjust the probe velocity independently of frequency and still be able to pinpoint its location within a convection cell at a known time when the lower wall temperature is, for example, at its temporal maximum. The free parameter is the initial position of the probe x_0 which may be set at time $t_0 = 0$.

For definiteness, we see that the lower surface temperature is at a maximum at $t = 2\pi k/\omega$, k any integer, while the horizontal maximum in temperature occurs at a cell boundary at $x = 2\pi k/a$. A probe beginning at x_0 and moving at a velocity V will arrive at the cell boundary after a time

$$t = \frac{\dfrac{2\pi k}{a} - x_0}{V}. \tag{4.13}$$

To arrange for the probe to perceive the maximum convective temperature at a time $t = 2\pi k/\omega$, we see that

$$x_0 = 2\pi k\left(\frac{1}{a} - \frac{V}{\omega}\right). \tag{4.14}$$

The desired intersection in time and space will occur after one complete cycle of oscillation when $k = 1$. Thus in equation (4.12) we let

$$x = 2\pi\left(\frac{1}{a} - \frac{V}{\omega}\right) + Vt. \tag{4.15}$$

It is desirable to fix the probe's initial location in this manner so that temporal and spatial effects on the probe's temperature may be separated. A similar result could have been accomplished if $x_0 = 0$, but then the interesting conjunction of thermal maxima occurs at $t = 0$, when the initial conditions dominate the solution.

Equation (4.8) is similar to that investigated in [5] and [6]. However, rather than using a stability criterion, the procedure here is to integrate numerically the second order system governing the time dependent Fourier coefficients x_n. The velocity and temperature fields may then be reconstructed as a function of time to enable direct comparison between the analytical predictions and experimental results.

The problem was solved on the UCLA IBM 360/90 System, using Hammings predictor corrector method. It was discovered that at $\omega = 3$ or less, the fourth term in the series was always more than two orders of magnitude smaller than the first, so the series was truncated at three. In no case ($\omega < 20$) were more than six terms required.

During the course of the numerical investigations, various initial conditions were used. At low frequency, $\omega = 1$, the choice of initial conditions was found not to significantly influence the results, as the amplitudes x_n tended to change rapidly in a time small compared to one period whatever conditions were chosen. The procedure finally used was to initiate the run with white noise of amplitude 10^{-3} at a time during the oscillation cycle when the Rayleigh number is just passing critical in the linear, unmodulated sense ($R_c = 27\pi^4/4$).

The low frequency numerical results agree with those in [5] in the sense that for a given set of boundary conditions, the percentage change in critical Rayleigh number will follow curves similar to those on Figs. 1–3, provided the periodicity or amplitude criterion is applied. It should be mentioned that [6] uses fixed boundary conditions, while [4] and [5] use free boundary conditions, but the results are quite close if plotted according to the percentage change in the appropriate critical Rayleigh number. Therefore, the free-free boundary conditions are assumed throughout this analysis.

Despite these points of agreement between this and previous analyses, the system (4.8) fails to duplicate the experimental results described in Section 3. For example, at $\omega = 1$, $\varepsilon = 1$, $R_m \cong 1{\cdot}2R_c$, the amplitudes x_n grow to a magnitude of 10^5 during the part of the cycle when the instantaneous Rayleigh number is supercritical, then decay when $R < R_c$ to their initial value. Although one is technically correct in describing such behavior as marginally stable according to the periodicity condition, the linear assumptions are clearly invalid. Further, it does not seem reasonable to describe a state where large amplitude convection occurs as being marginally stable.

Using linear theory, one cannot duplicate the temperature traces recorded by the moving probe in the experimental program. The heart of the discrepancy is the unbounded exponential growth which results from the linear approximation. This growth is manifested in two ways, illustrated in Figs. 16 and 17. In Fig. 16 the disturbance has grown so large that a temperature larger than that at either boundary results. If a lower mean Rayleigh number is chosen, a more subtle discrepancy arises. While a physically plausible profile appears in Fig. 17, a comparison with Fig. 11, taken under similar boundary conditions, gives a clue to the problem. In the experimental trace, the disturbance grows rapidly to some finite amplitude, then remains

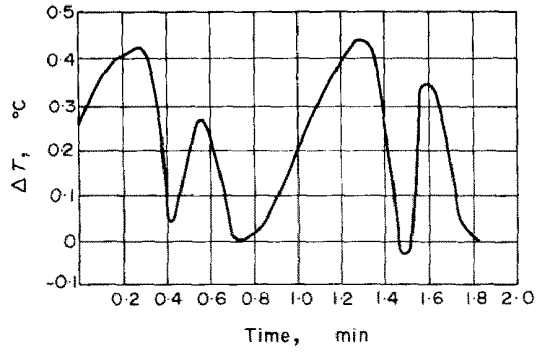

FIG. 16. Computed temperature trace at $z = 0{\cdot}5$, $R_{\min} = 0$, $R_{\max} = 1440$, $\varepsilon = 1$, $\omega = 3$.

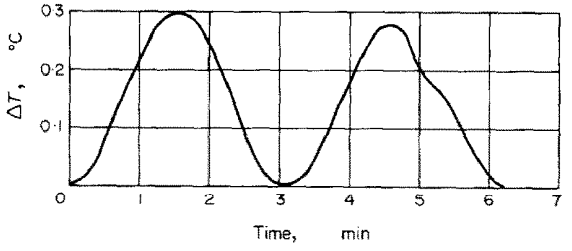

FIG. 17. Computed temperature trace at $z = 0{\cdot}5$, $R_{\min} = 0$, $R_{\max} = 1054$, $\varepsilon = 1$, $\omega = 1$.

at that general size until it rapidly disappears. This results in a uniform depression at the peak of the cycle. On the other hand, the linear theory gives a qualitatively different behavior wherein convection persists at a Rayleigh number when the experiment shows motion has ceased. The type of skewed profile seen in Fig. 17 is not observed in the experimental data.

To provide an analytical description of the observed experimental flows, the energy relations are derived from the equations of motion. If we define

$$T = \bar{T} + \theta_1,$$

$$u = \frac{\partial \psi}{\partial z}, \quad w = \frac{\partial \psi}{\partial x}, \quad v = 0$$

where $\bar{T}$ is the mean or horizontally averaged temperature, θ_1 is the departure from the mean so that $\bar{\theta}_1 = 0$, and ψ is the nondimensional stream function. The momentum equation in the Boussinesq approximation may be written

$$\frac{1}{Pr}\left[\frac{\partial}{\partial t}\nabla^2\psi + \frac{\partial \psi}{\partial z}\frac{\partial}{\partial x}\nabla^2\psi - \frac{\partial \psi}{\partial x}\frac{\partial}{\partial z}\nabla^2\psi\right] = \nabla^4\psi - R\frac{\partial \theta_1}{\partial x}. \quad (4.16)$$

The mean temperature equation, which is derived by horizontally averaging the energy conservation equation, is

$$\frac{\partial \bar{T}}{\partial t} - \frac{\partial}{\partial z}\left(\overline{\theta_1 \frac{\partial \psi}{\partial x}}\right) = \frac{\partial^2 \bar{T}}{\partial z^2}. \quad (4.17)$$

The remaining terms in the heat-conduction equation govern θ_1

$$\frac{\partial \theta_1}{\partial t} + \frac{\partial \psi}{\partial x}\frac{\partial \theta_1}{\partial x} - \frac{\partial \psi}{\partial x}\frac{\partial \theta_1}{\partial z} + \frac{\partial}{\partial z}\left(\overline{\theta_1 \frac{\partial \psi}{\partial x}}\right) - \frac{\partial \psi}{\partial x}\frac{\partial \bar{T}}{\partial z} = \nabla^2\theta_1. \quad (4.18)$$

Separating the mean temperature $\bar{T}$

$$\bar{T} = \bar{T}_0 + \bar{\theta}_2, \quad (4.19)$$

where $\bar{\theta}_2$ represents the contribution of convection and $\bar{T}_0$ is given by (2.14), we have for $\bar{\theta}_2$

$$\frac{\partial \bar{\theta}_2}{\partial t} - \frac{\partial}{\partial z}\left(\overline{\theta_1 \frac{\partial \psi}{\partial x}}\right) = \frac{\partial^2 \bar{\theta}_2}{\partial z^2}. \quad (4.20)$$

We now multiply equation (4.16) by ψ, (4.18) by θ_1, and (4.20) by $\bar{\theta}_2$ and integrate over the volume of the field, assuming the motion is in the form of two dimensional rolls of period $2\pi/a$. It may be shown that the resultant relations are

$$\frac{1}{2Pr}\frac{\mathrm{d}}{\mathrm{d}t}\iint\left[\left(\frac{\partial \psi}{\partial x}\right)^2 + \left(\frac{\partial \psi}{\partial z}\right)^2\right]\mathrm{d}x\,\mathrm{d}z = R\iint\frac{\partial \theta_1}{\partial x}\psi\,\mathrm{d}x\,\mathrm{d}z - \iint\left[\frac{\partial^2 \psi}{\partial z^2} + \frac{\partial^2 \psi}{\partial z^2}\right]^2\mathrm{d}x\,\mathrm{d}z \quad (4.21)$$

$$\tfrac{1}{2}\frac{\mathrm{d}}{\mathrm{d}t}\iint\theta_1^2\,\mathrm{d}x\,\mathrm{d}z - \iint\frac{\mathrm{d}\bar{T}}{\mathrm{d}z}\frac{\partial \psi}{\partial x}\theta_1\,\mathrm{d}x\,\mathrm{d}z = -\iint\left[\left(\frac{\partial \theta_1}{\partial x}\right)^2 + \left(\frac{\partial \theta_1}{\partial z}\right)^2\right]\mathrm{d}x\,\mathrm{d}z \quad (4.22)$$

$$\tfrac{1}{2}\frac{\mathrm{d}}{\mathrm{d}t}\int\bar{\theta}_2^2\,\mathrm{d}z + \int\frac{\partial \bar{\theta}_2}{\partial z}\left(\overline{\theta_1 \frac{\partial \psi}{\partial x}}\right)\mathrm{d}z = -\int\left(\frac{\partial \theta_2}{\partial z}\right)^2\mathrm{d}z. \quad (4.23)$$

The limits of integration are 0 to 1 on z and 0 to $2\pi/a$ on x. To these points the energy relations are exact. Following Stuart [12], we use the shape assumption, presuming that the fundamental convection mode has the same shape as that predicted by linear theory. It is further assumed that the harmonics are sufficiently smaller than the fundamental that they may be ignored. This latter assumption restricts the validity of the approach to low frequency of modulation. We let

$$\begin{aligned}\psi &= \frac{1}{a}A(t)\cos ax\sin\pi z\\ \theta_1 &= B(t)\sin ax\sin\pi z\\ \theta_2 &= C(t)\sin 2\pi z\end{aligned} \quad (4.24)$$

so that we have free-free rolls and heat conduction only at the boundaries. A differential equation for C is derived by substituting (4.24) into (4.23), giving

$$\frac{\mathrm{d}C}{\mathrm{d}t} + \frac{\pi}{2}AB = -4\pi^2 C. \quad (4.25)$$

Using (4.21), we can derive the following expression for A:

$$\frac{\mathrm{d}A}{\mathrm{d}t} = -Pr\left((a^2+\pi^2)A - \frac{RBa^2}{(a^2+\pi^2)}\right). \quad (4.26)$$

Finally, to solve for B we use (4.22). We also use the low frequency approximation for the stationary thermal gradient:

$$\frac{\partial \bar{T}_0}{\partial z} = -(1+\varepsilon\cos\omega t) \quad (4.27)$$

so that

$$\frac{\partial \bar{T}}{\partial z} = -(1+\varepsilon\cos\omega t) + 2\pi C\cos 2\pi z. \quad (4.28)$$

This leads to the relation governing B:

$$\frac{dB}{dt} = -B(a^2+\pi^2)+A(1+\varepsilon\cos\omega t)+\pi AC. \quad (4.29)$$

Equations (4.25), (4.26), and (4.29) are now integrated numerically to solve for the time dependent convection within the fluid layer.

If one sets $\varepsilon = 0$, $d/dt = 0$, it is possible to solve for the steady state amplitude of the unmodulated problem. One finds

$$w = -\frac{\partial\psi}{\partial x}$$

$$= 2\pi(2a^2+2)^{1/2}\left[\frac{R-R_c}{R_c}\right]^{1/2}\sin ax\sin\pi z \quad (4.30)$$

in agreement with the second order results of Malkus and Veronis [13] and Segel [14]. With $\varepsilon = 0$, $d/dt \neq 0$, the numerical integration gives the temperature sensed by the moving probe during the onset of convection. Results of this integration are presented in Fig. 18, which is seen to be in qualitative agreement with the experimental trace in Fig. 10.

The numerical investigation of the energy equations is conducted in a manner analogous to the experimental program described in Section 3. A series of cases are examined, over the experimental range of variables, $0 < \varepsilon < 1$, $0 < \omega < 1$. A parametric presentation of the results is given in Section 5, and some typical curves are depicted in Figs. 19 and 20. Figure 19 has exactly the same boundary conditions as Fig. 17 and should be compared to the experimental curve in Fig. 11. One sees that the onset of observable convection is qualitatively correct in Fig. 19. In Fig. 20, many of the qualitative features of the experimental evidence in Section 3 are duplicated. One sees distortion of the mean at points A and B, and typical updraft and downdraft patterns at C and D. The probe velocity in this figure has been adjusted so that cell boundaries are encountered at the peak of the lower wall temperature at C and D. The origin of the asymmetry at D and other salient features of this curve are discussed in Section 3.

A significant departure from the periodicity type behavior is observed in the solution of the energy relations. At low frequency ($\omega = 1$) the convection amplitude does not grow over several cycles of oscillation when the mean Rayleigh number is supercritical from the linear, periodicity point of view. Instead, the energy relations predict that the amplitude of convection is the same at the peak of the first cycle of oscillation as on succeeding cycles. This is found to be true for $0{\cdot}2 < \varepsilon < 1{\cdot}0$, $1{\cdot}2\,R_c < R_{mean} < 5\,R_c$, where $R_c = 657$. This conclusion is fully supported by the experimental data, where the convection time constant always appears to be smaller than a cycle of oscillation at $\omega = 1$.

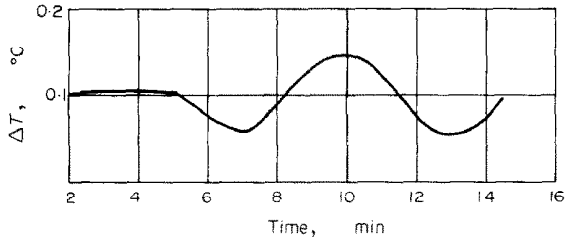

FIG. 18. Computed onset of convection with no modulation, $R = 750$, $z = 0{\cdot}5$.

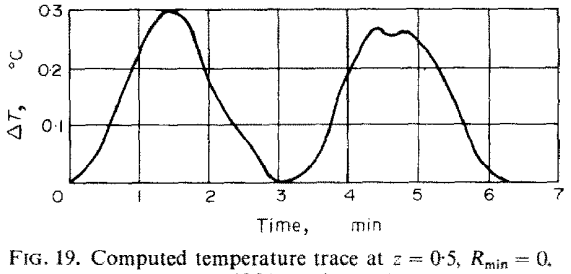

FIG. 19. Computed temperature trace at $z = 0{\cdot}5$, $R_{min} = 0$, $R_{max} = 1054$, $\varepsilon = 1$, $\omega = 1$.

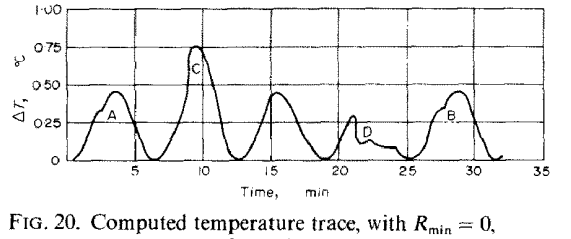

FIG. 20. Computed temperature trace, with $R_{min} = 0$, $R_{max} = 1450$, $\varepsilon = 1$, $\omega = 0{\cdot}5$.

5. CORRELATIONS AND CONCLUSIONS

In this section we present a parametric summary of the experimental and analytical data compiled during the project. The experimental data is given in two ranges of modulation amplitude, rather than at discrete values of ε. Since ε is defined in terms of the imposed mean temperature gradient, it is not possible to vary ε independently. In the first range, $0{\cdot}3 < \varepsilon < 0{\cdot}5$, while in the second, $0{\cdot}85 < \varepsilon < 1$. The experimental results are plotted with respect to $R_c = 1708$, while for the numerical curves $R_c = 658$. In Fig. 21, instances of observable convection, defined as a 5 per cent distortion of the basic profile are indicated by ●, while ○ indicates no motion or distortion of the conduction profile. The curve labeled I is the amplitude criterion from [5] for $\varepsilon = 0{\cdot}3$, while curve II is from the same source but for $\varepsilon = 0{\cdot}5$. The curve labeled III is derived from the analysis of Section 4 and represents the boundary of observable motion at $\varepsilon = 0{\cdot}5$.

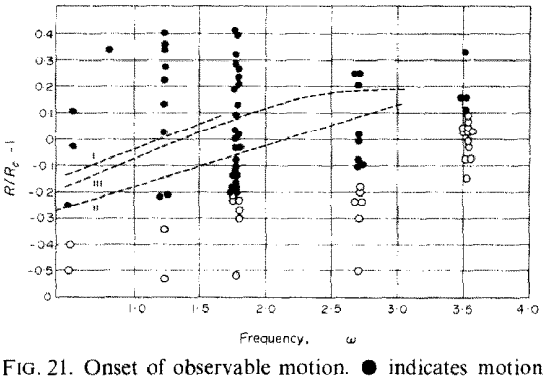

FIG. 21. Onset of observable motion. ● indicates motion observed; ○ indicates conduction only. $0{\cdot}3 < \varepsilon < 0{\cdot}5$.

The quasi-steady criterion (2·7) gives values for (R/R_c-1) as $-0{\cdot}23$ and $-0{\cdot}33$ for $\varepsilon = 0{\cdot}3$ and $\varepsilon = 0{\cdot}5$, respectively.

Figure 21 shows positive evidence of stabilization at $\omega = 3{\cdot}5$. The states indicated by these high frequency experimental points are stable by any of the criteria discussed. Stated simply, no convection occurs even though the mean Rayleigh number is nearly 10 per cent higher than that required to produce well defined convection rolls in the unmodulated case.

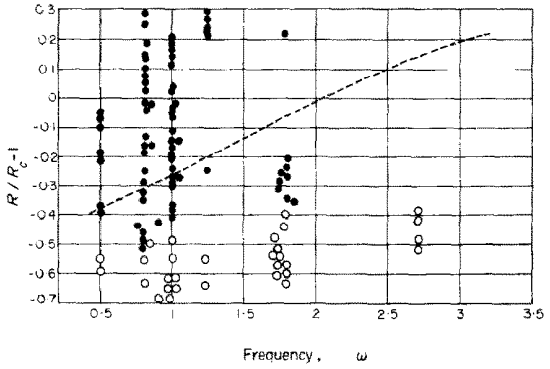

FIG. 22. Onset of observable motion. ● indicates motion observed; ○ indicates conduction only. $0{\cdot}8 < \varepsilon < 1{\cdot}0$.

Figure 22 is similar to Fig. 21 except that $0{\cdot}85 < \varepsilon < 1$. For this case, the quasi-steady criterion (2.7) gives values of (R/R_c-1) of $-0{\cdot}44$ and $-0{\cdot}50$ for $\varepsilon = 0{\cdot}8$ and $1{\cdot}0$, respectively. The dashed curve is derived from the numerical integration of the energy relations in Section 4. There is very little variation with ω in the experimental data as compared to Fig. 21. Since the data at a given frequency were all taken together, this effect would not appear to be ascribable to error in technique or measurement. The theoretical curve, on the other hand, shows strong frequency dependence. An explanation for this evident conflict is not readily apparent. Unfortunately, it was impossible to obtain large amplitude data at $\omega \sim 3$, as discussed in Section 3, and to see whether stabilization might occur for higher frequency. In this context, it should be mentioned that Yih and Li [15], investigating a problem for which upper and lower surface temperatures are modulated 180° out of phase, have found that, although stabilization occurs for low values of ε, destabilization can occur for larger values of ε.

In Figs. 23 and 24, an attempt has been made to correlate the experimental data to the periodicity criteria in [5] and [6]. In these figures, ● represents a flow in which evidence of convection appears over the entire cycle of oscillation, while ○ indicates conduction only exists at some point in the cycle. One presumes that if a state is unstable in a periodicity sense, convection will eventually spread to the entire cycle. It should be mentioned that the determination of stability in this sense involves considerable subjective judgment, as it is often difficult to separate convection from conduction at high Rayleigh number, particularly at low frequency.

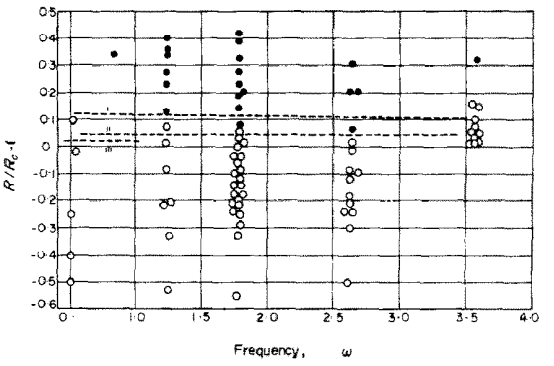

FIG. 23. ● indicates convection occurs over entire cycle of oscillation; ○ indicates convection has ceased at some point in the cycle. $0{\cdot}3 < \varepsilon < 0{\cdot}5$.

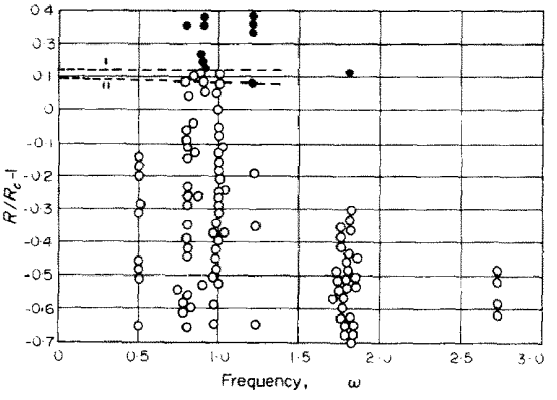

FIG. 24. ● indicates convection occurs over entire cycle of oscillation; ○ indicates convection has ceased at some point in the cycle. $0{\cdot}8 < \varepsilon < 1{\cdot}0$.

In Fig. 23, the curve I is the periodicity criterion from [5], $\varepsilon = 0{\cdot}5$; II is [5], $\varepsilon = 0{\cdot}3$, and III is [6], $\varepsilon = 0{\cdot}4$. It should be recalled that curve III is the fixed wall case (as is the data), while I and II have the free-free boundary condition. The difference between free and fixed boundaries, on a percentage basis, is seen to be smaller than the experimental scatter.

In comparing Figs. 21 and 23, it can be seen that the periodicity and amplitude criteria merge at about $\omega = 3$, for $0{\cdot}3 < \varepsilon < 5$. This is in agreement with the results of Rosenblat and Herbert [5]; see also Fig. 3. Under the conditions $\omega = 3{\cdot}5$, $0{\cdot}3 < \varepsilon < 0{\cdot}5$, a given flow is either all conduction or all convection. At high frequency, low amplitude, convection sets in nearly simultaneously over the whole cycle.

In Fig. 24, I is from [5], $\varepsilon = 1$; II is from [6], $\varepsilon = 1$. Again, the scarcity of data at high frequency does not allow evaluation of frequency effects.

Figure 25 shows the maximum amplitude of convection temperature difference measured as a function of $R_{max}-R_c$ at a frequency $\omega = 1$. It can be seen that this amplitude correctly follows the theoretical quasi-steady $(R-R_c)^{1/2}$ dependence. On the other hand, the higher frequency data in Fig. 26, $\omega = 2{\cdot}72$ and $\omega = 1{\cdot}8$, shows considerable scatter and is closer to a linear dependence on $R-R_c$. At high frequency one should not expect the quasi-static approximation to be valid.

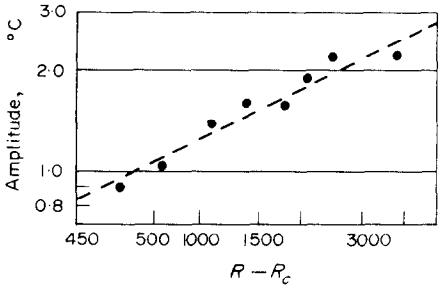

FIG. 25. Convection amplitude as a function of $R-R_c$, with $\omega = 1$.

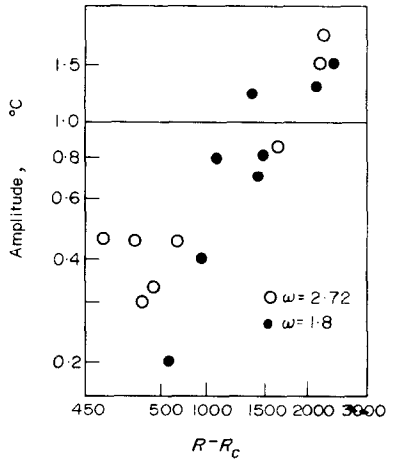

FIG. 26. Convection amplitude as a function of $R-R_c$, at higher frequencies.

5.1. *Concluding remarks*

Although the frequency range studied was rather severely restricted, the experimental and theoretical data are seen to support the previous analytical work, particularly the amplitude condition results of Rosenblat and Herbert [5]. Although apparently of interest in determining the onset of continuous convection, the periodicity condition does not describe the onset of observable motion in the fluid at low frequency. At $\omega = 3$, the two conditions merge, with the periodicity condition then properly defining the stability limit at $\omega > 3$.

Acknowledgement—The authors wish to acknowledge the invaluable advice of Dr. J. Whitehead concerning the experimental apparatus. This work was supported, in part, by the N.S.F. through grant GA-31247.

REFERENCES

1. R. J. Donnelly, Experiments on the stability of viscous flow between rotating cylinders—III. Enhancement of stability by modulation, *Proc. R. Soc.* **A281**, 130–139 (1964).
2. R. J. Donnelly, F. Reif and H. Suhl, Enhancement of hydrodynamic stability by modulation, *Phys. Rev. Lett.* **9**, 363–365 (November 1962).
3. R. Thompson, Instabilities of some time dependent flows, Ph.D. Department of Meteorology, Massachusetts Institute of Technology, Cambridge, Massachusetts (June 1968).
4. G. Venezian, Effect of modulation on the onset of thermal convection, *J. Fluid Mech.* **35**, 243–254 (February 1969).
5. S. Rosenblat and D. M. Herbert, Low-frequency modulation of thermal instability, *J. Fluid Mech.* **43**, 385–398 (August 1970).
6. S. Rosenblat and G. A. Tanaka, Modulation of thermal convection instability, *Physics Fluids* **14**, 1319–1322 (July 1971).
7. G. M. Homsy, Global stability of time-dependent flows—2. Modulated fluid layers, *J. Fluid Mech.* **62**, 387–403 (January 1974).
8. S. H. Davis, Convection in a box: linear theory, *J. Fluid Mech.* **30**, 465–478 (November 1967).
9. W. G. Spangenberg and W. R. Rowland, Convective circulation in water induced by evaporative cooling, *Physics Fluids* **4**, 743–750 (June 1961).
10. I. G. Currie, The effect of heating rate on the stability of stationary fluids, *J. Fluid Mech.* **29**, 337–347 (August 1967).
11. S. Chandrasekhar, *Hydrodynamic and hydromagnetic stability*. Oxford University Press, London (1961).
12. J. T. Stuart, On the non-linear mechanics of hydrodynamic stability, *J. Fluid Mech.* **4**, 1–21 (January 1958).
13. W. V. R. Malkus and G. Veronis, Finite amplitude cellular convection, *J. Fluid Mech.* **4**, 225–260 (July 1958).
14. L. A. Segel, Distant side walls cause slow amplitude modulation of cellular convection, *J. Fluid Mech.* **38**, 203–224 (August 1969).
15. C.-S. Yih and C.-H. Li, Instability of unsteady flows or configurations—2. Convective instability, *J. Fluid Mech.* **54**, 143–152 (1972).

NAISSANCE D'INSTABILITES DANS UNE COUCHE FLUIDE CHAUFFEE SINUSOÏDALEMENT PAR LE DESSOUS

Résumé—Le problème étudié concerne l'effet de la modulation thermique sur la stabilité d'une couche fluide chauffée par le dessous. Une expérience a été réalisée dans laquelle une couche d'air est soumise à un chauffage sinusoïdal autour d'une valeur moyenne non nulle. Une analyse numérique des équations de stabilité linéaire a montré que l'hypothèse de linéarité n'est pas valable aux faibles fréquences de modulation étudiées expérimentalement. Une analyse non-linéaire utilisant l'hypothèse de forme et des conditions aux limites libres a été développée et traitée numériquement. On a trouvé, à la fois analytiquement et expérimentalement, qu'aux faibles fréquences la modulation est destabilisante, tandis qu'aux fréquences plus élevées une certaine stabilisation apparait.

INSTABILITÄTSBEGINN IN EINER SINUSFÖRMIG VON UNTEN BEHEIZTEN FLÜSSIGKEITSSCHICHT

Zusammenfassung—Es wird der Einfluß thermischer Modulation auf die Stabilität einer von unten beheizten Flüssigkeitsschicht untersucht. In einem Experiment wurde eine Luftschicht einer sinusförmigen Beheizung um einen Mittelwert unterworfen. Eine numerische Analyse der linearen Stabilitätsgleichung zeigte, daß die Linear-Annahme ungültig ist für die kleinen experimentell untersuchten Modulationsfrequenzen. Eine nichtlineare Analyse mit Annahmen über die Form und freie Begrenzung wurde entwickelt und numerische überprüft. Es ergab sich sowohl experimentell wie auch analytisch, daß für geringe Frequenzen die Modulation destabilisierend wirkt, während für höhere Frequenzen ein Stabilisierungseffekt auftritt.

ВОЗНИКНОВЕНИЕ НЕУСТОЙЧИВОСТИ В СЛОЕ ЖИДКОСТИ, НАГРЕВАЕМОЙ СИНУСОИДАЛЬНО СНИЗУ

Аннотация — Исследуется эффект тепловых колебаний на устойчивость слоя жидкости, нагреваемой снизу. Эксперимент проводился в воздушном слое, подверженном синусоидальному нагреву в пределах среднего ненулевого значения. Численный анализ линейных уравнений устойчивости показал, что допущение линейности является неприемлимым при низких частотах колебаний, изученных экспериментально. Разработан и реализован численно нелинейный анализ для определенной геометрической формы и заданных условиях на свободной границе. Как экспериментально, так и теоретически найдено, что при низких частотах колебания являются дестабилизирующими, в то время как при высоких частотах очевидна некоторая устойчивость.